We are IntechOpen,
the world's leading publisher of
Open Access books
Built by scientists, for scientists

4,800
Open access books available

122,000
International authors and editors

135M
Downloads

Our authors are among the

154
Countries delivered to

TOP 1%
most cited scientists

12.2%
Contributors from top 500 universities

BOOK CITATION INDEX
CLARIVATE ANALYTICS
INDEXED

WEB OF SCIENCE™

Selection of our books indexed in the Book Citation Index
in Web of Science™ Core Collection (BKCI)

Interested in publishing with us?
Contact book.department@intechopen.com

Inverse Approach for Calculating Temperature in Thermal Elasto-Hydrodynamic Lubrication of Line Contacts

Li-Ming Chu[1], Hsiang-Chen Hsu[1], Jaw-Ren Lin[2] and Yuh-Ping Chang[3]
[1]Department of Mechanical and Automation Engineering, I-Shou University,
[2]Department of Mechanical Engineering, Nanya Institute of Technology,
[3]Department of Mechanical Engineering, Kun Shan University,
Taiwan

1. Introduction

It is well known by now that pressure, temperature, and film shape definitely play important roles in the failure of heavily loaded non-conformal contacts, such as rolling element bearings, gears, traction drives, or cams and tappets. Furthermore, the effect of heat generated due to the shearing of the high-pressure lubricant is no longer negligible under sliding conditions, as the heat changes the characteristics of the oil flow because of a decrease in viscosity. Therefore, the thermal effect on the film thickness and traction is significant in elastohydrodynamic lubricated contacts. So an accurate estimate of the temperature distribution in the contact zone at various operational parameters is necessary.

Since (Sternlicht et al., 1961) started to consider the thermal effects of line contact in the EHL under rolling/sliding conditions, the inclusion of thermal effects in EHL has been an important subject of research in the field of tribology. Many numerical solutions considering the thermal effects on EHL have been presented, for instance, by (Ghosh & Hamrock, 1985), (Salehizadeh & Saka, 1991), and (Lee & Hsu, 1993); and for thermal point contact problems by (Zhu & Wen, 1984), (Kim & Sadeghi, 1992), and (Lee & Hsu, 1995). With respect to measuring the temperature increase in EHL contacts, (Cheng & Orcutt, 1965), (Safa et al., 1982), and (Kannel et al., 1978) have measured the temperature increase in a sliding surface using a thin film gauge deposited on a disc. (Turchina et al., 1974) and (Ausherman et al., 1976) employed an improved infrared technique to measure the temperature distribution of the oil film and surface. They demonstrated that the temperature was maximum at zones with minimum film thickness in the contact side lobes. Recently, (Yagi et al., 1966) described the mechanism of variations of EHL oil film under high slip ratio conditions. The oil film thickness between a ball surface and a glass disk was measured using optical interferometry, and the temperature of both the surfaces and of the oil film average across it were measured using an infrared emission technique. They demonstrated that the shape of the oil film can be varied by viscosity wedge action which related to pressure and temperature.

During the last decade, optical interferometry has been found to be the most widely used and successful method in measuring oil film. Several studies of an EHL film were carried

out by experiments (Cameron & Gohar, 1966; Foord et al., 1968; Johnston et al., 1991; Gustafsson et al., 1994; Yang et al., 2001). Since the image processing technique requires a calibration, which always introduces errors, the multi-channel interferometry method was proposed by (Marklund et al., 1998) to overcome such problems. (Luo et al., 1996) measured the center lubricated film thickness on point contact EHL by using a relative optical interference intensity technique. Furthermore, (Hartl et al., 1999) presented a colorimetric interferometry to improve over conventional chromatic interferometry in which film thickness is obtained by color matching between interferogram and color-film thickness dependence obtained from Newton rings for static contact.

When the film thickness map is obtained from the optical interferometry, the pressure distribution can be computed by using the elastic deformation and the force balance theories. This pressure can be used in the Reynolds equation to evaluate the viscosity. (Paul & Cameron, 1992) used an impact viscometer to evaluate the pressure distribution and the apparent viscosity. (Wong et al., 1992) measured the apparent viscosity, the shear stress, and shear rate of liquid lubricants using an impact viscometer. Moreover, they developed a new viscosity-pressure relationship which takes the form of a Barus equation at low pressures and reaches a limiting viscosity at high pressure. (Astrom & Venner, 1994) presented a combined experimental/numerical approach to gain insight into such pressure fluctuations. They used the film thickness map obtained by (Gustafsson et al., 1994) to calculate the pressure distribution from the force balance and elastic deformation theories in a grease-lubricated point contact. (Östensen et al., 1996) theoretically investigated the possibility of using optical interferometry for determining pressure and apparent viscosity in an EHL point contact. Results showed that some of the small fluctuations in pressure are due to the discontinuities in film thickness. However, this small pressure fluctuation would result in a large error in calculating the viscosity due to the amplification by the performing pressure differentiation in the Reynolds equation. Hence, (Lee et al., 2002) developed an inverse approach to overcome this problem in EHL line contacts. In this algorithm, only a few measured points of film thickness are sufficient enough to estimate the pressure distribution without any fluctuation.

Recently, an inverse model proposed by (Yang, 1998) has been widely applied in many design and manufacturing problems in which some of the surface conditions cannot be measured. However, this method used in the inverse TEHL (thermal elastohydrodynamic lubrication) problem is still scarce in the literature. Hence, in this paper, the inverse approach is extended to calculate the mean oil film temperature rise and surface temperature rise distributions and to investigate the sensitivity of the temperature rise and the apparent viscosity for the experimental measurement errors. Moreover, the 'exact' solutions, such as pressure, temperature rise and film thickness are obtained from the numerical solution of the TEHL line contacts problem.

3. Theoretical analysis

As shown in Fig. 1, the contact geometry of two rollers can be reduced to the contact geometry as a roller and a flat surface.

For the steady state, thermal EHL line contact problems, the Reynolds equation can be expressed in the following dimensionless form as:

$$\frac{\partial}{\partial X}\left(\frac{\bar{\rho}H^3}{\bar{\eta}} \frac{\partial P}{\partial X} \right) = \lambda \frac{\partial}{\partial X}(\bar{\rho}H) \tag{1}$$
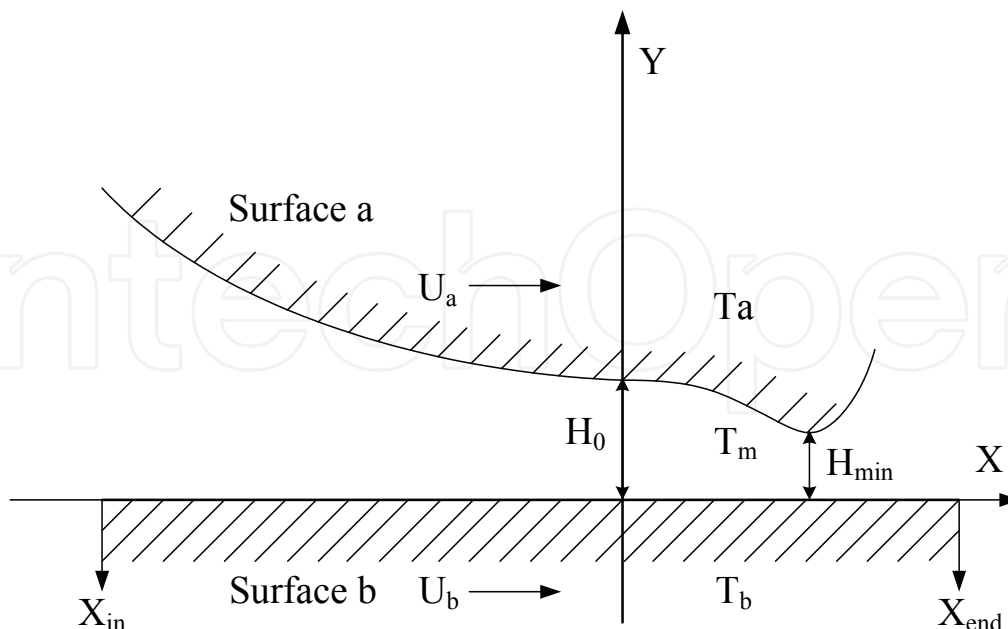
Fig. 1. The geometry of an EHL line contact.

where

$$\lambda = \frac{12\eta_0 \bar{u} R^2}{b^3 p_h}$$

In this equation, the mass density and the viscosity of lubricants related to pressure and temperature can be expressed as:

$$\bar{\rho} = \frac{\rho}{\rho_0} = \left[1 + \frac{0.6 \times 10^{-9} p}{1 + 1.7 \times 10^{-9} p} \right] [1 - \beta(T_m - T_0)] \tag{2}$$

$$\bar{\eta} = \exp\{(9.67 + \ln\eta_0)[-1 + (1 + 5.1 \times 10^{-9} p)^z] - \gamma(T_m - T_0)\} \tag{3}$$

where z is the pressure-viscosity index, β is thermal expansivity of lubricant, γ is temperature-viscosity coefficient of lubricant. If the pressure and mean temperature are given, the apparent viscosity and density can be calculated from equations (2) and (3), respectively.

3.1 Pressure calculation
It has been known that the film thickness in an EHL contact is the sum of the elastic deformation of the surfaces and the gap distance between two rigid surfaces. In the EHL line contact, the film shape in the dimensionless form is given as:

$$H_i = H_0 + \frac{X_i^2}{2} - \frac{1}{\pi} \int_{X_{in}}^{X_{end}} P(X) \ln|X - X| \, dX \tag{4}$$

Discretizing the domain with equi-distant mesh size Δ, Eq. (4) can be approximated by

$$H_i - \frac{X_i^2}{2} - H_0 = -\frac{1}{\pi}\sum_{j=1}^{n} K_{ij}P_j \tag{5}$$

where

$$K_{ij} = \left(i - j + \frac{1}{2}\right)\Delta\left[\left(\ln\left|i - j + \frac{1}{2}\right|\Delta\right) - 1\right] - \left(i - j - \frac{1}{2}\right)\Delta\left[\left(\ln\left|i - j - \frac{1}{2}\right|\Delta\right) - 1\right] \tag{6}$$

The normal load for the line contact is assumed to be constant, thus the constant H_0 can be obtained from the dimensionless force balance equation as:

$$\int_{X_{in}}^{X_{end}} P(X)\,dX = \frac{\pi}{2} \tag{7}$$

or in the discretized form

$$\frac{\pi}{2} = \Delta\sum_{j=1}^{n} P_j \tag{8}$$

Once the film shape is measured, the pressure distribution can be calculated from Eqs (5) and (8) or in a matrix form as:

$$\mathbf{H} = \mathbf{DP} \tag{9}$$

or

$$\begin{Bmatrix} H_i - \dfrac{X_i^2}{2} \\ \pi/2\Delta \end{Bmatrix} = \begin{bmatrix} -\dfrac{1}{\pi}K_{ij} & 1 \\ 1 & 0 \end{bmatrix} \begin{Bmatrix} P_j \\ H_0 \end{Bmatrix} \tag{10}$$

This system equation consists of n+1 equations and unknowns, and the matrix D is a full square matrix. In this paper, if the pressure distribution is calculated from this system equation, then it is called the direct inverse method.

3.2 Inverse approximation for calculating pressure
In order to avoid the small fluctuation in calculating the pressure, the pressure distribution can be assumed to be a polynomial function, the pressure distribution can be represented in the following series form in terms of X as:

$$P_j = \sum_{m=0}^{l} a_m(X_j - c)^m = \sum_{m=0}^{l} a_m f_{jm} \tag{11}$$

where a_m is an undetermined coefficient, l is a positive integer, and c is a constant. In this paper, most of c is set to zero. Substituting this approximation into the system Eq. (10), the governing equation becomes

$$\mathbf{H} = \mathbf{DFA} \tag{12}$$

or

$$\left\{ \begin{matrix} H_i - \dfrac{X_i^2}{2} \\ \pi/2\Delta \end{matrix} \right\} = \begin{bmatrix} -\dfrac{1}{\pi}K_{ij} & 1 \\ 1 & 0 \end{bmatrix} \begin{bmatrix} f_{jm} & 0 \\ 0 & 1 \end{bmatrix} \left\{ \begin{matrix} a_m \\ H_0 \end{matrix} \right\} \tag{13}$$

In this equation, Hi is the film thickness with n measured point, and D is a $(n+1)\times(k+1)$ matrix, where k is the total node number of the pressure. It is obvious that F is a $(k+1)\times(l+2)$ matrix, and A is a $(l+2)$ vector. For the viscous EHL problem, it has been known that the pressure spike appears in the dimple region of the film shape. Hence, to obtain the pressure distribution using the inverse approach, it is necessary to divide the domain into a few regions due to the singular point at the pressure spike. Therefore, the divided matrix form can be written as:

$$\left\{ \begin{matrix} [H_i - \dfrac{X_i^2}{2}]_1 \\ \bullet \\ \bullet \\ \bullet \\ [H_i - \dfrac{X_i^2}{2}]_N \\ \pi/2\Delta \end{matrix} \right\} = \left[\begin{matrix} [-\dfrac{1}{\pi}K_{ij}]_1 & & \begin{matrix}1\\ \bullet\\ \bullet\\ \bullet\\ 1\end{matrix} \\ \bullet & & \\ \bullet & & \\ \bullet & & \\ [-\dfrac{1}{\pi}K_{ij}]_N & & \\ [1\ \bullet\ \bullet\ \bullet\ 1] & & 0 \end{matrix} \right] \begin{bmatrix} [f_{jm}]_1 & [0] & [0] & [0] & [0] & [0] \\ [0] & \bullet & [0] & [0] & [0] & [0] \\ [0] & [0] & \bullet & [0] & [0] & [0] \\ [0] & [0] & [0] & \bullet & [0] & [0] \\ [0] & [0] & [0] & [0] & [f_{jm}]_N & [0] \\ [0] & [0] & [0] & [0] & [0] & 1 \end{bmatrix} \left\{ \begin{matrix} [a_m]_1 \\ \bullet \\ \bullet \\ \bullet \\ [a_m]_N \\ H_0 \end{matrix} \right\} \tag{14}$$

If the unknown variables a_m and H_0 are given, the estimated film thickness can be calculated from Eq. (14). It is obvious that the estimated film thickness is different from the measured one. Hence, to obtain the smallest error between the measured and estimated film thickness, the linear least squares methods is employed here. The least-squares criterion requires the following function to be minimized.

$$g = (\mathbf{H}^{\text{estimated}} - \mathbf{H}^{\text{measured}})^{\text{T}}(\mathbf{H}^{\text{estimated}} - \mathbf{H}^{\text{measured}}) \tag{15}$$

The best value for A can be determined from

$$\frac{\partial g}{\partial \mathbf{A}} = 0 \tag{16}$$

Then, the governing equation for the best value of A can be obtained as

$$\mathbf{A} = \left[(\mathbf{DF})^{\text{T}}(\mathbf{DF}) \right]^{-1} (\mathbf{DF})^{\text{T}}\mathbf{H} \tag{17}$$

In this equation, $(\mathbf{DF})^{T}(\mathbf{DF})$ is a $(l+2)\times(l+2)$ matrix. As a result, it can save much computation time in calculating A because l is generally less than 20 in the present study. The variables a_m are given, the pressure distribution can be calculated from Eq. (11). Furthermore, since the pressure has been expressed as the polynomial form, the small fluctuation in the pressure can be eliminated.

3.3 Temperature calculation

The temperature distribution within an oil film can be solved by the energy equation subject to appropriate boundary conditions. Neglecting heat convection across the film and

circumferential conduction in the film, the energy equation for line contact problems may be written as:

$$\frac{\partial}{\partial y}\left[\kappa\frac{\partial T}{\partial y}\right] = \rho c_p u\frac{\partial T}{\partial x} - \eta\left(\frac{\partial u}{\partial y}\right)^2 - T\beta u\frac{\partial p}{\partial x} \tag{18}$$

Adding the continuity equation to Eq. (18) and integrating the resultant energy equation across the film thickness can be expressed as:

$$\rho c_p\int_0^h(\frac{\partial uT}{\partial x} + \frac{\partial vT}{\partial y})\,dy = \kappa\frac{\partial T}{\partial y}\Big|_0^h + \int_0^h\eta\left(\frac{\partial u}{\partial y}\right)^2\,dy + \int_0^h T\beta u\frac{\partial p}{\partial x}\,dy \tag{19}$$

The non-linear integral convective terms in Eq. (19) can be linearized and be approximately equivalent to the product of the mean velocity and the temperature.

$$T_m = \frac{\dfrac{1}{h}\displaystyle\int_0^h uT\,dy}{\dfrac{1}{h}\displaystyle\int_0^h u\,dy} = \frac{\dfrac{1}{h}\displaystyle\int_0^h uT\,dy}{u_m} \tag{20}$$

Integration of the continuity equation across the film thickness can be expressed as:

$$\frac{\partial u_m h}{\partial x} = 0 \tag{21}$$

The substitution of Eqs. (20) and (21) into the energy equation leads to:

$$\rho c_p u_m h\frac{\partial T_m}{\partial x} = \frac{2k(T_a + T_b - 2T_m)}{h} + \beta u_m h T_m\frac{\partial p}{\partial x} + \frac{\eta u^{*2}}{h} + \frac{1}{12\eta}(\frac{\partial p}{\partial x})^2 h^3 \tag{22}$$

or in dimensionless form as:

$$\overline{\rho}U_m H^2\frac{\partial\overline{T}_m}{\partial X} = 2\xi(\overline{T}_a + \overline{T}_b - 2\overline{T}_m) + \Omega U_m H^2\overline{T}_m\frac{\partial P}{\partial X} + \Lambda\overline{\eta}U^{*2} + \frac{\Lambda\Phi^2 H^4}{12\overline{\eta}}(\frac{\partial P}{\partial X})^2 \tag{23}$$

where

$$\xi = \frac{k\eta_0 R}{\rho_0 c_p E'b^3}$$

$$\Omega = \frac{\beta p_h}{\rho_0 c_p}$$

$$\Lambda = \frac{E'R^3}{\rho_0 c_p b^3 T_0}$$

$$\Phi = \frac{p_h}{E'}(\frac{b}{R})^3$$

The energy equation requires the surface temperatures of the rollers as its boundary conditions. The problem of the surface temperature of a semi-infinite solid subjected to a moving heat source was first solved by Carslaw and Jaeger. Therefore, the boundary conditions for Eq. (23) can be expressed as:

$$\bar{T}_b(X,0) = \bar{T}_{b0} + \frac{\kappa\sqrt{b}}{T_0\sqrt{\pi\rho_b c_b k_b u_b}} \frac{T_0 R}{b^2} \int_{X_{in}}^{X} \frac{2(\bar{T}_m - \bar{T}_b)}{H} \frac{dX'}{\sqrt{X - X'}} \tag{24}$$

$$\bar{T}_a(X,1) = \bar{T}_{a0} + \frac{\kappa\sqrt{b}}{T_0\sqrt{\pi\rho_a c_a k_a u_a}} \frac{T_0 R}{b^2} \int_{X_{in}}^{X} \frac{2(\bar{T}_a - \bar{T}_m)}{H} \frac{dX'}{\sqrt{X - X'}} \tag{25}$$

$$\bar{T}_m = \bar{T}_0 \text{ , at } X = -\infty \tag{26}$$

Once the film shape is measured, the variables a_m can be calculated from Eq. (17). Therefore, the pressure distribution can be calculated from Eq. (11), and the estimated film thickness can be calculated from equation (14). As mentioned above, since the mass density and the viscosity of lubricants are the functions of the pressure and mean temperature, so the initial mean temperature must be guessed, and the Gauss-Seidel iteration is employed to calculate the temperature from Eqs. (2), (3) and (23)-(26). If the pressure distribution, film shape, mass density and viscosity of lubricants with are given, then the Reynolds Eq. (1) can be satisfied.

4. Results and discussion

4.1 Direct inverse method
In order to illustrate the validity of the present technique discussed above, several numerical tests have been performed. Typical results for the case of W=1.8182x10^{-5}, U=7.2727x10^{-12}, and G = 3500 with 169 grid points are shown in Figs. 2 and 3. In this study, the 'exact' solution of film thickness, pressure, and temperature rise distribution in the lubricated contact are calculated numerically by using the lubricant and roller properties according to Tables 1 and 2. In solving the thermal EHL line-contact problems, the coupled Reynolds, energy, load balance, film thickness, rheology, and surface temperature equations must be solved simultaneously.

When the measured points are the same as the estimated points, it is not necessary to use the series form to represent the pressure distribution. Hence, the solution obtained from Eqs. (2), (3), (9) and (23)-(26) are called the solution of the direct inverse method. By using the direct inverse method, Fig. 2 shows the effect of the measured points of the film thickness on the pressure distribution, and Fig. 3 shows the effect of the measured points of the film thickness on the temperature rise distribution. In these figures, the input data is the film thickness at different measured points. It is obvious that with increasing the number of measured points, the solution approaches the 'exact' numerical solution. When the 8-point measurements are taken uniformly, results show that the estimated values of the pressure and temperature rise are bad in the whole region. When the 43-point measurements are taken uniformly, results show that the estimated values of the pressure and temperature rise are quite accurate in the inlet and outlet regions, but the pressure and temperature rise spikes are incorrect. When the measured points are increased, results show that the estimated values of the pressure and the temperature rise become quite accurate in the pressure spike region. It is clear that the direct inverse method requires a lot of measured points.
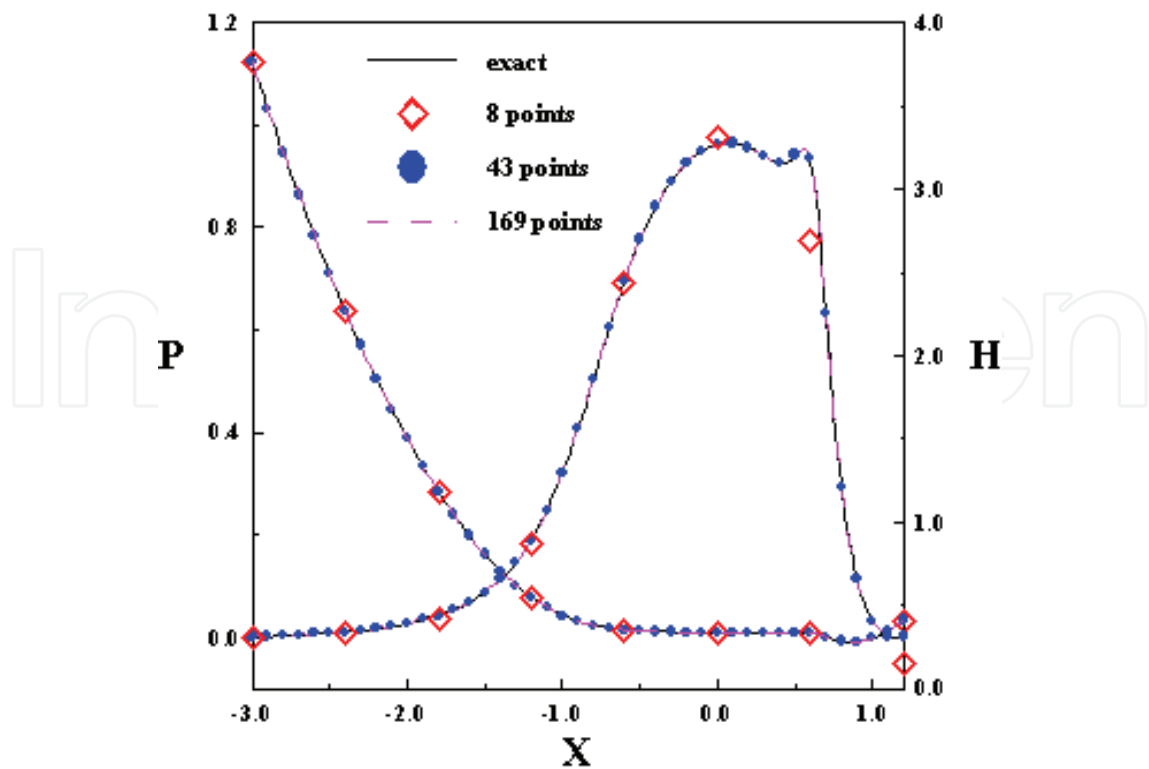
Fig. 2. Pressure distributions for different measured points in the film thickness using direct inverse method.
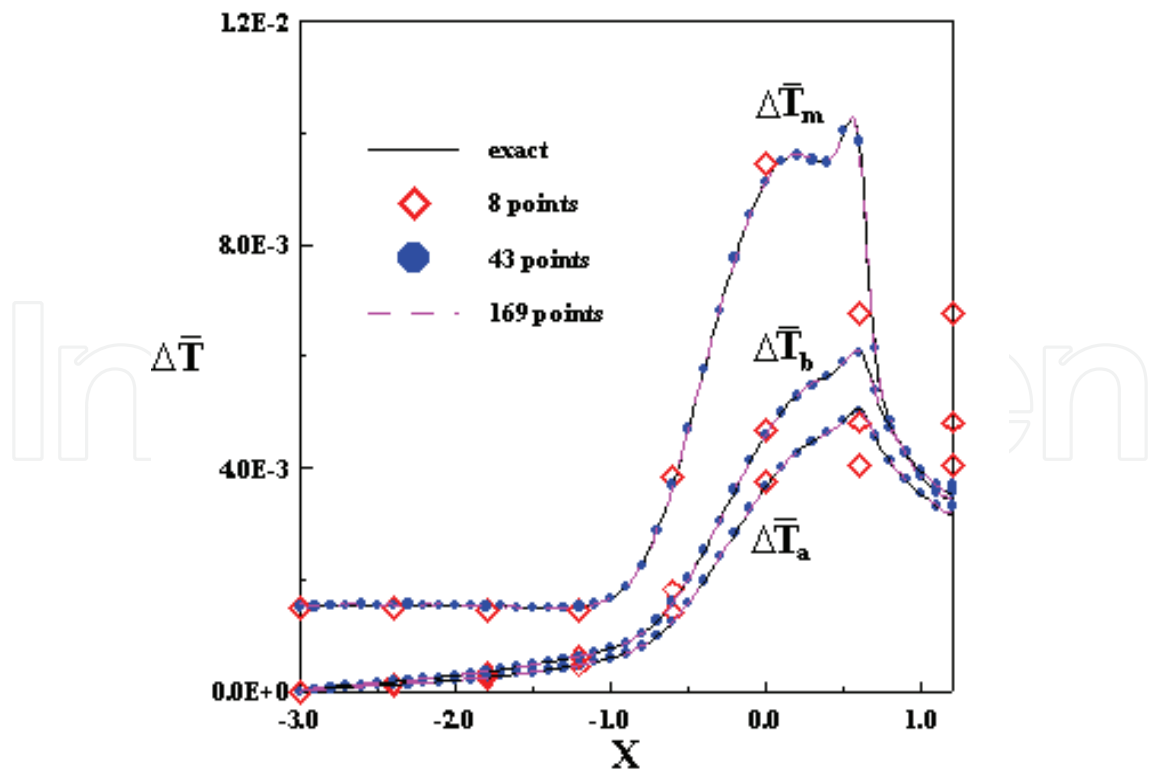

Fig. 3. Temperature rise distributions for different measured points in the film thickness using direct inverse method.

G (Material parameter)	3500.0
Inlet temperature of lubricant, K	313.0
Inlet viscosity of lubricant, Pa-S	0.04
Inlet density of lubricant, kg/m³	846.0
Pressure viscosity coefficient, 1/GPa	15.91
Temperature-viscosity coefficient, 1/K	6.4×10^{-4}
Thermal conductivity of lubricant, W/m-K	0.14
Specific heat of lubricant, J/Kg-K	2000.0
Pressure-viscosity coefficient (Roelands)	0.4836

Table 1. Properties of lubricant.

Equivalent radius, m	0.02
Thermal conductivity of rollers, W/m-K	47.0
Specific heat of rollers, J/Kg-K	460.0
Density of rollers, kg/m³	7850.0
Elastic modulus of rollers, GPa	200
Poisson's ratio of rollers	0.3

Table 2. Properties of rollers.

Usually, the measurement error always occurs in the optical interferometry measurement. This minor measurement error makes the estimation away from the 'exact' numerical solution. In this study, the measured film thickness is generated from the pre-selected 'exact' numerical film thickness with the minor measurement error, and it can be expressed as:

$$H_i^{measured} = H_i^{exact} + \sigma H_c \lambda_i \tag{27}$$

where λ_i is a random number, H_c is the dimensionless central film thickness, and σ is the dimensionless standard deviation of the measurement error. Figs. 4 and 5 show the effect of the dimensionless standard deviation of the measurement error on the pressure and temperature rise distribution. It is seen from these figures that the minor measurement error on the oil film significantly influences the pressure and temperature rise distribution. Table 3 also shows that the resolution in film thickness can result in an error in the solution of the pressure and temperature rise distribution. Generally, the film thickness gradient is sensitive to the pressure distribution. As a result, pressure fluctuations can be found everywhere. If this pressure distribution is used to solve the temperature rise distribution, the error in the temperature rise should be also found everywhere.
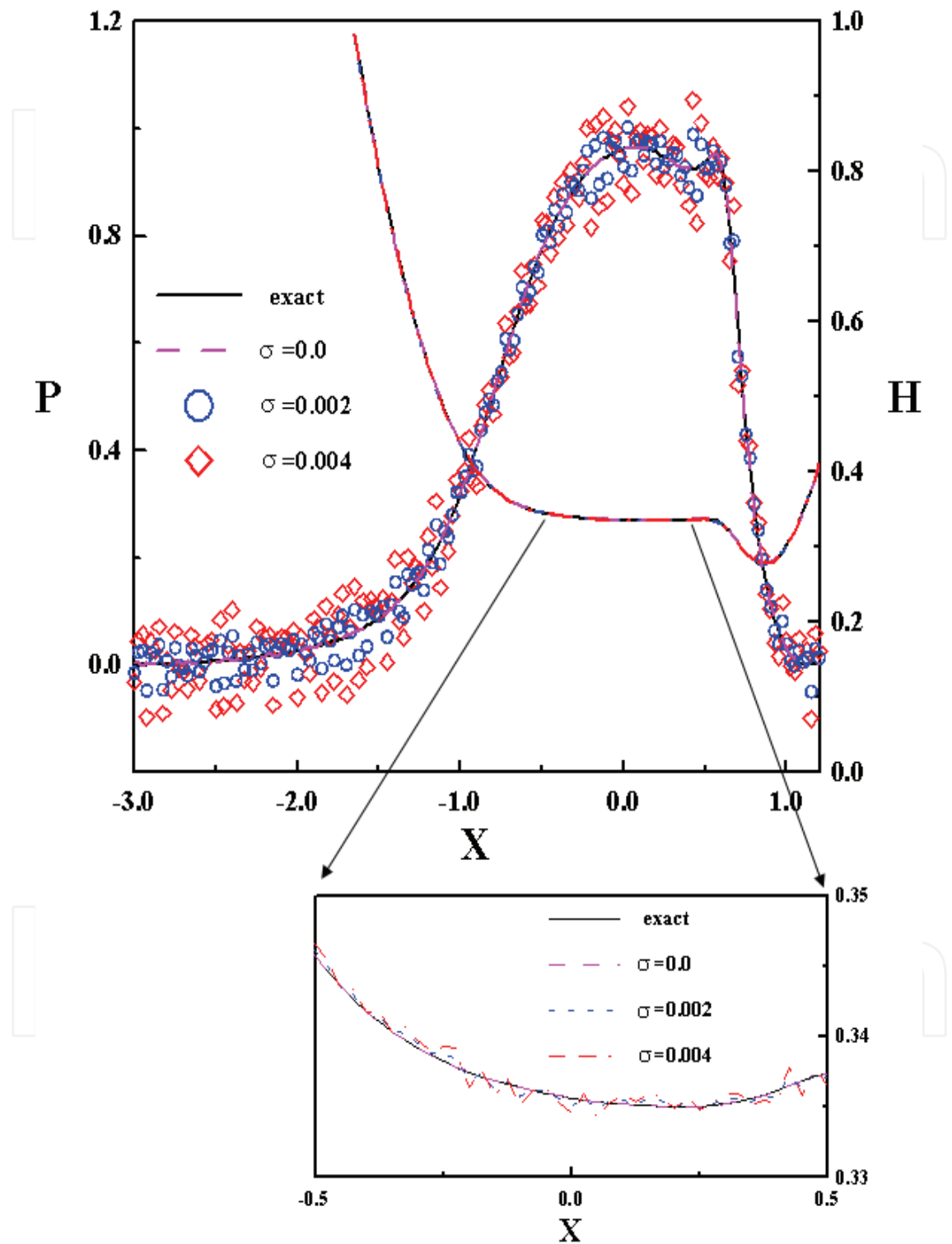
Fig. 4. Pressure distributions for different standard deviations of the measured errors with 169 measured points in the film thickness using direct inverse method.
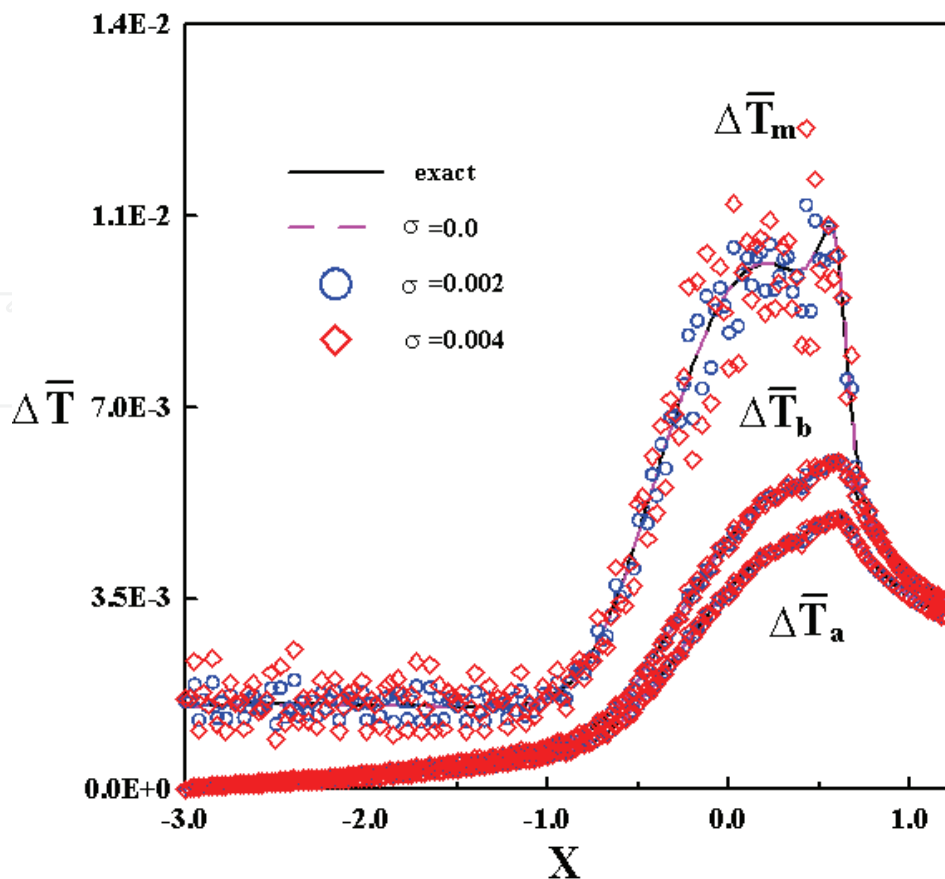
Fig. 5. Temperature rise distributions for different standard deviations of the measured errors with 169 measured points in the film thickness using direct inverse method.

standard deviation of the measured error		$\sigma = 0.002$	$\sigma = 0.004$	$\sigma = 0.006$
$(\dfrac{H^{measured} - H^{exact}}{H^{exact}})_{\max.}(\%)$		-0.230	-0.463	-0.693
$(\dfrac{P^{present} - P^{exact}}{P^{exact}})_{\max.}(\%)$	D.I.	77.467	153.541	229.362
	I.A.	2.355	4.061	5.309
$(\dfrac{\Delta T_m^{present} - \Delta T_m^{exact}}{\Delta T_m^{exact}})_{\max.}(\%)$	D.I.	-12.477	26.587	44.270
	I.A.	3.480	6.601	8.908
$(\dfrac{\Delta T_a^{present} - \Delta T_a^{exact}}{\Delta T_a^{exact}})_{\max.}(\%)$	D.I.	-3.240	7.205	13.283
	I.A.	1.797	3.833	5.571
$(\dfrac{\Delta T_b^{present} - \Delta T_b^{exact}}{\Delta T_b^{exact}})_{\max.}(\%)$	D.I.	-3.527	7.690	13.983
	I.A.	1.858	3.969	5.786

Table 3. Effect of film thickness measurement error on pressure and temperature ($-1 < X < 1$)

4.2 Inverse approach solution for pressure and temperature rise distributions

To overcome the problems of pressure and temperature rise fluctuations, this paper proposes the use of an inverse approach. It is known that a pressure spike appears in the dimple region of the film shape in the viscous EHL problems. Hence, to obtain accurate pressure and temperature rise distributions using the inverse approach, it is necessary to divide the domain into several regions due to the singular point at the pressure spike. In this paper, the domain is divided into three regions including the inlet region, the Hertz contact region, and the outlet region, respectively.

The unknown pressure distribution is approximated by a polynomial form shown in Eq. (11) with $c = -3$ and $a_0 = 0$; and the degrees of these three regions are shown in Table 4. The measured points in the film thickness can be chosen as 12, 21, and 31, within a domain from $X_{in} = -3$ to $X_{end} = 1.2$, and have been shown in Table 4. By using Eq. (17), the polynomial coefficients can be calculated. Substituting these coefficients into Eq. (11), the estimated pressure distribution can be calculated. It is seen from Figs. 6 and 7 that the number of measured points significantly influences the pressure and temperature rise distributions. With the increasing measured points, the solutions of the pressure and temperature rise distributions approach the 'exact' numerical solution. A twelve-point measurement in the film thickness gives a smooth solution of the pressure and temperature rise distributions, but it still exhibits a few errors on the whole region. For the 21 measured points in the film thickness, the solution of the pressure and temperature rise distributions are almost the same as the 'exact' numerical solution, but it still exhibits a few errors on the pressure and temperature rise in the vicinity of the spike region. Therefore, to obtain accurate pressure and temperature rise estimations, it is necessary to increase the number of measured points in the dimple region and in the pressure spike region, as shown in Fig. 6 and Table 4.

The minor measurement error on the oil film significantly influences the pressure and temperature rise distributions. Therefore, to understand the effect of pressure error on the film shape, the estimated film shape can be calculated from the calculated pressure using Eq. (14). It is seen from Fig. 6 that with a twelve-point measurement, the estimated film shape is a very smooth curve passed through the measured points, but it is different from the 'exact' numerical film shape within the domain from X=-3.0 to X=1.2. For the other two measured cases, the estimated film shape is quite close to the 'exact' numerical film shape. It was discussed above that any small error on the film shape could result in a significant error on the pressure and temperature rise distributions. Hence, with more measured points, the error in the estimated film shape can be reduced, so that the estimated pressure and temperature rise distributions can be closer to the 'exact' numerical solution.

The unknown pressure distribution is approximated by a polynomial form shown in equation (11) with the highest degree of 3, 5 and 7, respectively. It is seen from Figs. 8 and 9 that with the highest degree of 3, the inverse approach can simulate the pressure and temperature rise distributions, but the pressure and temperature rise slight oscillations occur at all regions, the error in the pressure and temperature rise are obvious and the pressure and temperature rise spikes disappear. With increasing polynomial degree, the errors in the pressure and temperature rise decrease.

It was discussed in Figs. 4 and 5 that the minor measurement error in the film thickness can result in pressure and temperature rise fluctuations everywhere. To obtain a smooth curve in the pressure and temperature rise distributions, the inverse approach is employed to solve this case. Figs. 10 and 11 present typical results obtained using the inverse approach when all the operating parameters are the same as those used in Figs. 4 and 5. In these

Item \ Region	I	II	III
X-range	-3.00≦X<-1.00	-1.0≦X<1.0	1.0≦X<1.2
Degrees	7	7	6
Measured points	-3.000 -2.750 -2.500 -2.250 -2.000 -1.750 -1.500 -1.250 -1.025	-1.000 -0.750 -0.500 -0.250 0.000 0.250 0.400 0.425 0.450 0.475 0.500 0.525 0.550 0.625 0.700 0.775 0.850 0.925	1.000 1.075 1.150 1.200

Table 4. The regions and measured points in the film thickness.
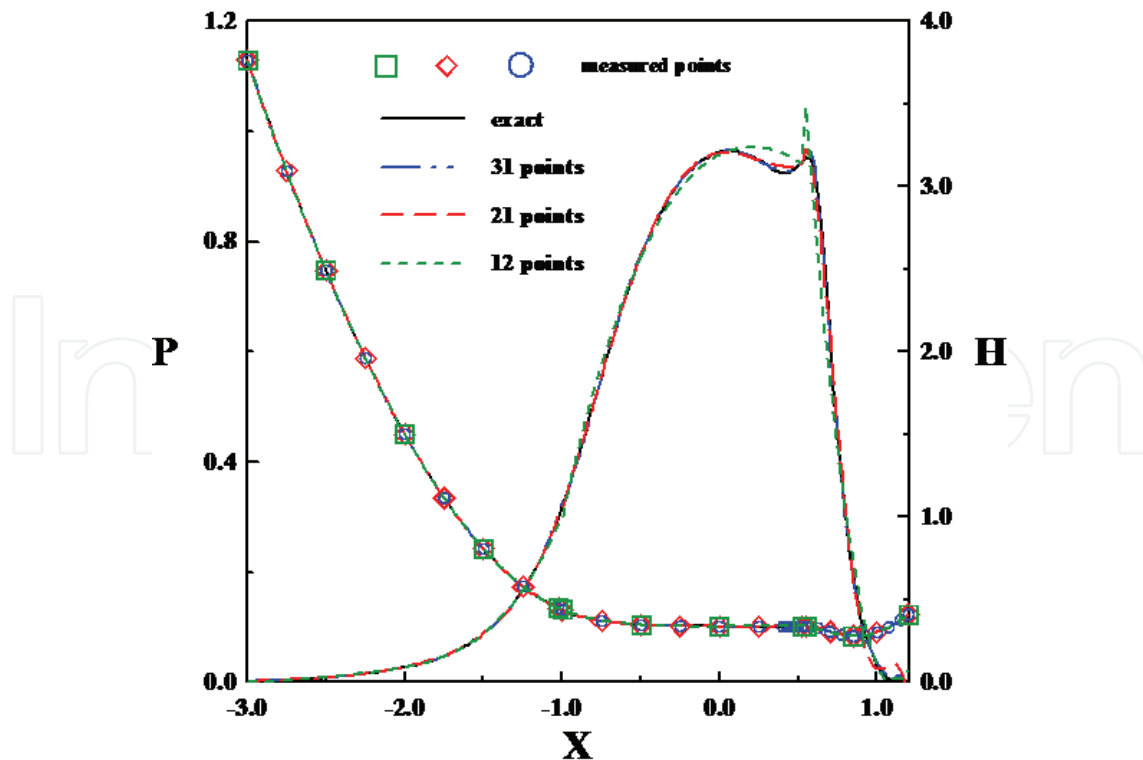
Fig. 6. Pressure distributions and film shapes for different measured points in the film thickness using inverse approach.
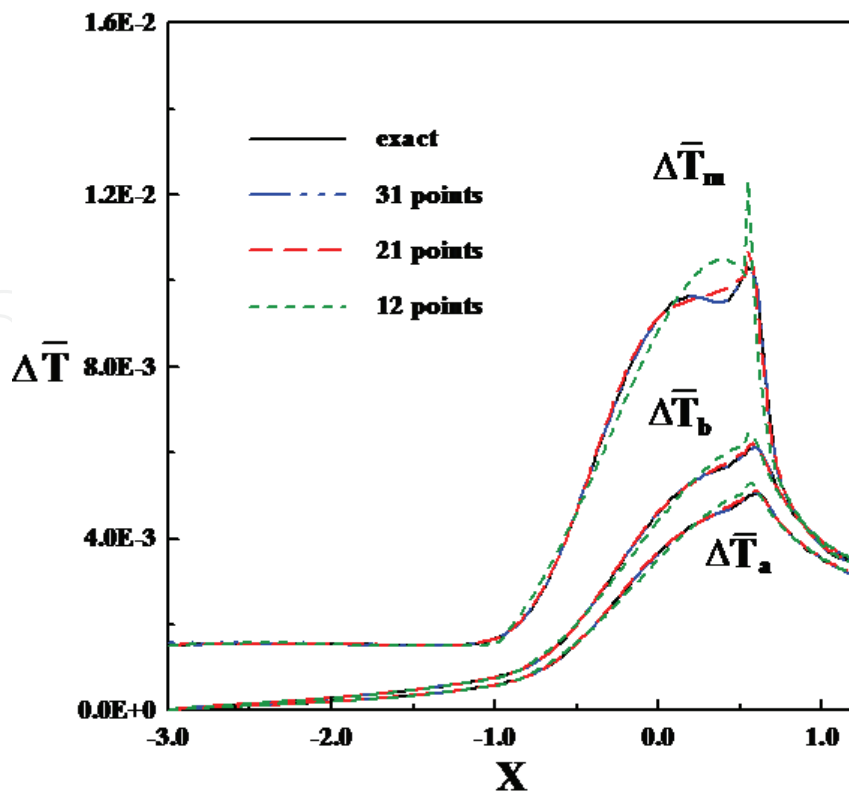
Fig. 7. Temperature rise distributions for different measured points in the film thickness using inverse approach.
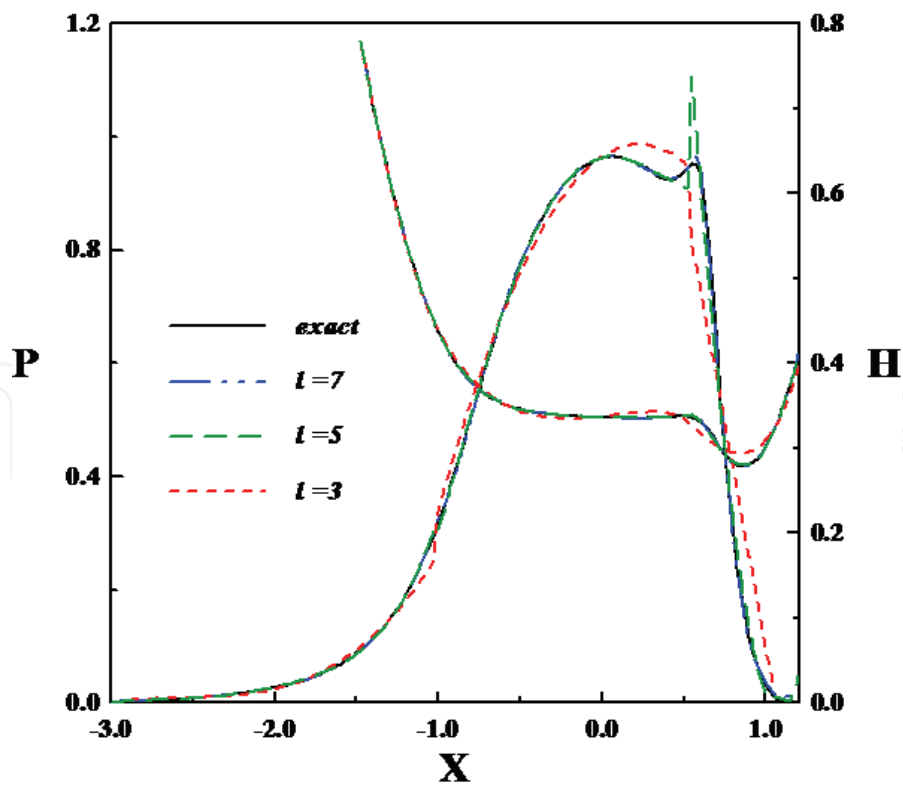
Fig. 8. Pressure distributions and film shapes for different degrees with 31 measured points in the film thickness using inverse approach.
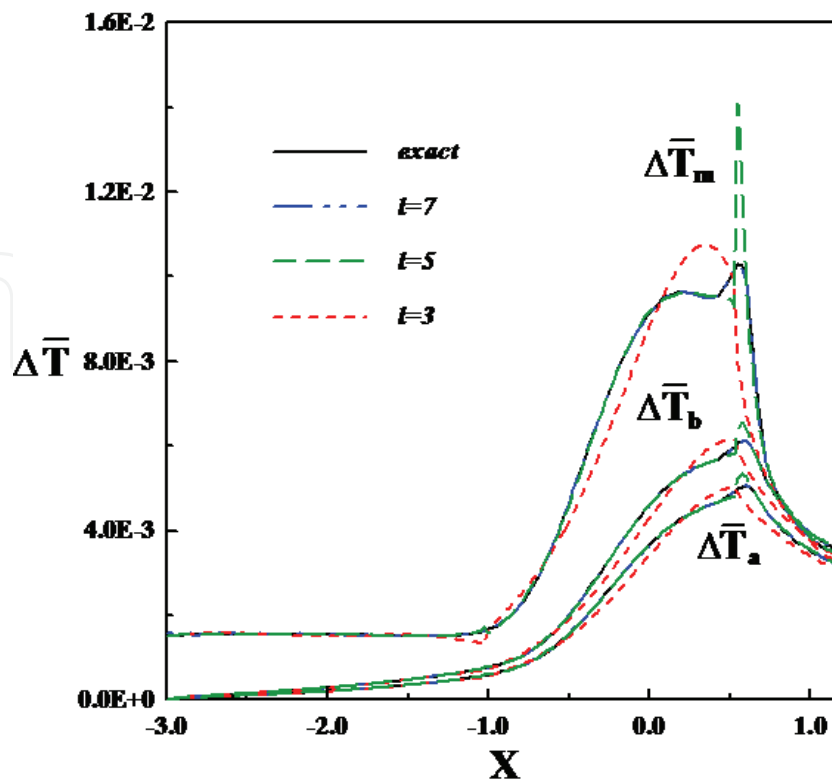
Fig. 9. Temperature rise distributions for different degrees with 31 measured points in the film thickness using inverse approach.

figures, the domain for the estimated pressure and temperature is divided into three regions with a total of 31 measured points in the film thickness. The range, degree of the polynomial form, and distribution of the measured points across these three regions are shown in Table 4. The numerical test tries to overcome the pressure and temperature rise fluctuations resulting from the implemented error in the film thickness. It is seen from Figs. 10 and 11 that with the increasing dimensionless standard deviation of the measurement error, the errors in the pressure and temperature rise distributions also increase, especially at the Hertz contact region. For the case of $\sigma = 0.002$, the results in the pressure and temperature rise distributions are almost equal to the 'exact' numerical solution. These results indicate that the present algorithm can overcome the pressure and temperature rise fluctuations due to the measurement error in the film thickness. Moreover, computing time can be saved due to the small matrix used in Eq. (17).

4.3 Inverse solution for apparent viscosity

Once the film shape is measured, the pressure distribution and estimated film thickness can be calculated from Eqs. (11), (14), and (17). As mentioned in section 3.3, the temperature rise distribution is calculated from Eqs. (2), (3) and (23)-(26) by using the Gauss-Seidel iteration. Furthermore, the mass density and the apparent viscosity of lubricants can also be obtained. Fig. 12 shows the dimensionless apparent viscosity versus the X-coordinate for various simulated measurement errors in the film thickness. The results show that the present algorithm still gives a reasonable solution for the apparent viscosity. By contrast, use of the
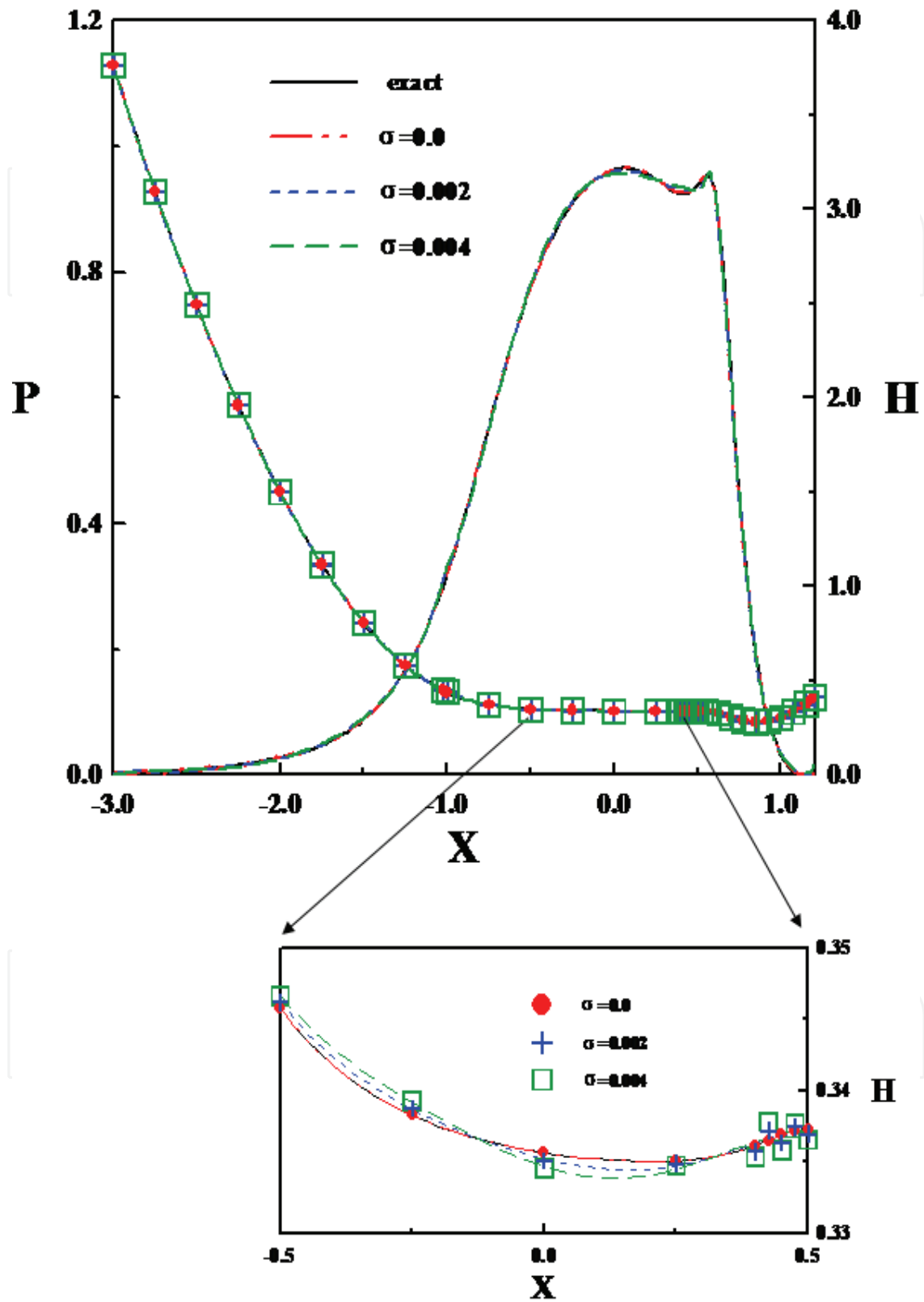
Fig. 10. Pressure distributions and film shapes for different standard deviations of the measured errors with 31 measured points in the film thickness using inverse approach.
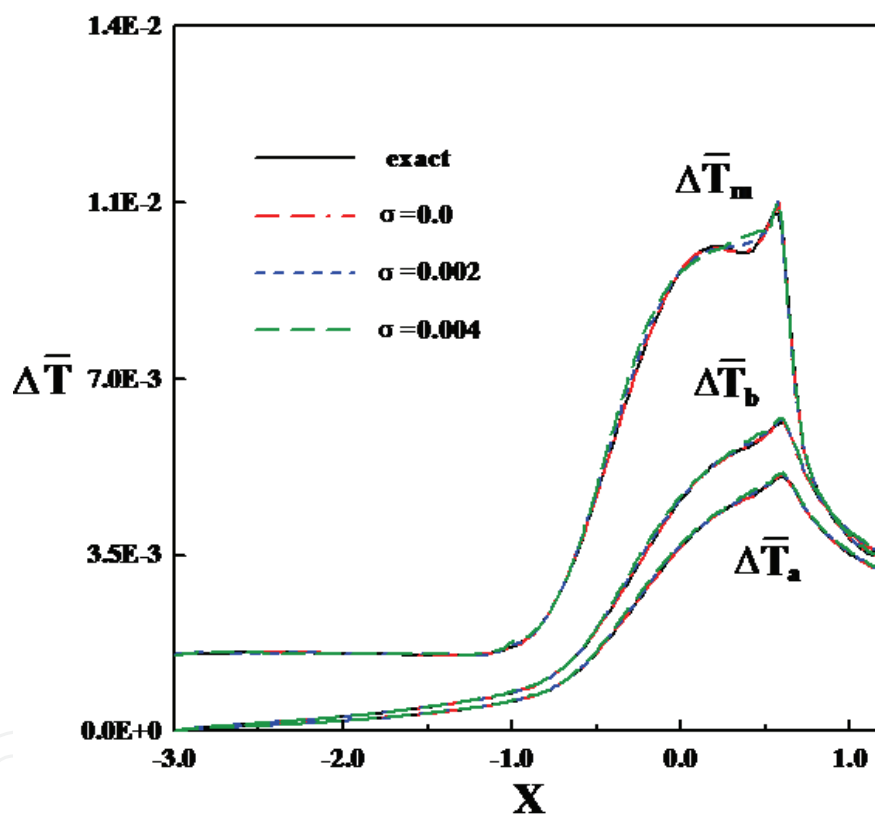
Fig. 11. Temperature rise distributions for different standard deviations of the measured errors with 31 measured points in the film thickness using inverse approach.
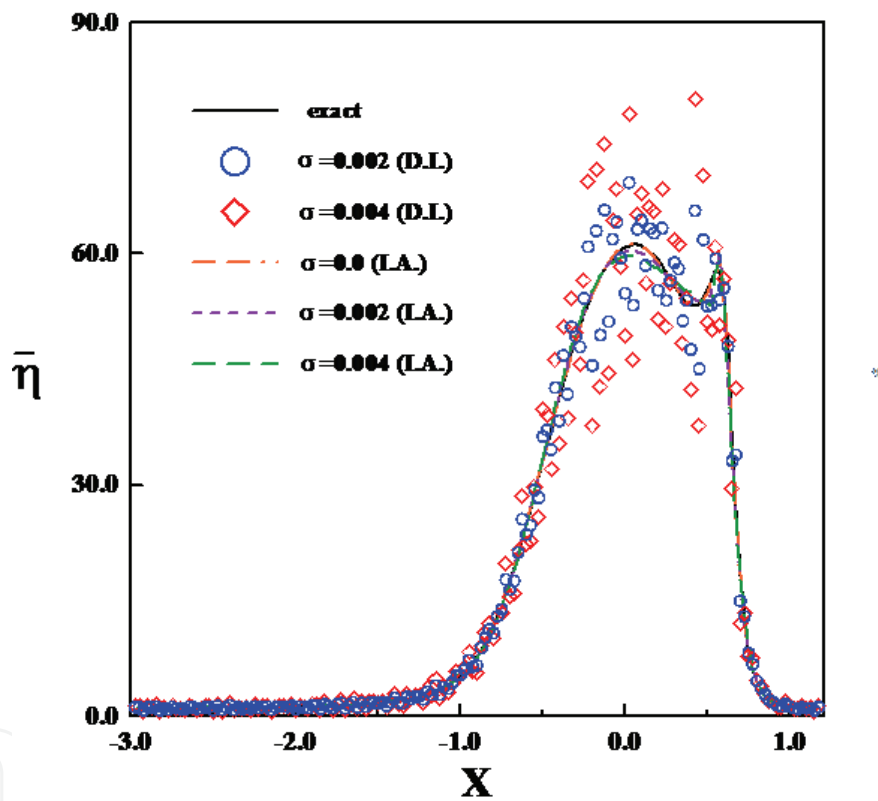
Fig. 12. Comparison of dimensionless apparent viscosity between two algorithms with implemented errors.

direct method results in much greater errors in the apparent viscosity results, especially in the Hertz contact region. This is the consequence of the pressure fluctuation mentioned in Section 4.1. However, in the present algorithm, when an implemented error occurs in the film shape, the estimated film shape can be obtained by using Eq. (14). Hence, the present algorithm provides a smooth curve not only in the pressure distribution, but also in the estimated film shape. Therefore, it produces much more accurate apparent viscosity results. However, the error in the apparent viscosity increases with the increasing standard deviation of the implemented error.

5. Conclusions

This paper describes an inverse approach to estimate the pressure distribution, the temperature rise distribution, and the apparent viscosity distribution in an EHL line contact if the film thickness is given. To obtain an accurate pressure, it is necessary to divide the domain into several regions due to the singularity at the pressure spike. The principle to choose the measured points is proposed. This approach overcomes the problems of pressure and temperature rise fluctuations and generates accurate results of the pressure and temperature rise distribution from a small number of measured points of film thickness, which also saves computing time. The conclusions from the main results can be summarized as follows:

1. The direct inverse method requires a lot of measured points of film thickness to establish the amplitude and location of the pressure and temperature spikes, but the inverse approach can obtain accurate results with only 31 measured points.
2. With the measurement error from the resolution in the film thickness measurement, this approach also presents a smooth curve of the pressure and temperature distributions with a small error in the inlet, pressure spike, and outlet regions.
3. Without the measurement error in the film thickness, this approach provides quite good solution for apparent viscosity. With the minor measurement error in the film thickness, this approach still gives a quite good solution in apparent viscosity, but the direct method provides much larger error in apparent viscosity.

6. Nomenclature

b semiwidth of hertzian contact (m)

c_p specific heat of the lubricant (J kg^{-1} K^{-1})

c_a, c_b specific heat of rollers a and b (J kg^{-1} K^{-1})

E' equivalent Young's modulus(Pa)

G dimensionless material parameter, $\alpha E'$

H dimensionless film thickness, hR/b^2

Hc dimensionless central film thickness

H_0 dimensionless constant defined in Eq. (4)

K_{ij} discretized kernel in Eq. (5)

k thermal conductivity of lubricant (W m^{-1} K^{-1})

k_a, k_b thermal conductivity of rollers a and b (W m^{-1} K^{-1})

p pressure (Pa)

p_h maximum hertzian pressure (Pa)

P dimensionless pressure, p/p_h

R equivalent radius of contact (m)

T temperature (K)

T_m mean temperature of lubricant film (K)

T_a, T_b surface temperature of rollers a and b

$\bar{T}$ dimensionless temperature, T/T_o

u_a, u_b surface velocity of rollers a and b (m s^{-1})

$\bar{u}$ average rolling velocity (m s^{-1})

U dimensionless speed parameter, $\eta_0 \bar{u} / E'R$

w load per unit width (N m^{-1})

W dimensionless load, W= $w / E'R$

x,y coordinate (m)

X,Y dimensionless coordinate, X=x/b, Y=y/h,

z Roelands' pressure-viscosity index

Δx or Δ distance between two neighboring grid points

η viscosity of lubricant (Pa-s)

η_0 viscosity of lubricant at ambient pressure and inlet lubricant (Pa-s)

$\bar{\eta}$ dimensionless viscosity, η / η_0

λ dimensionless viscosity parameter, $\lambda = 12\eta_0 \bar{u} R^2 / b^3 p_h$

λ_i random number

ρ density of lubricant (kg m^{-3})

ρ_0 inlet density of lubricant (kg m^{-3})

ρ_a, ρ_b density of rollers a and b (kg m^{-3})

$\bar{\rho}$ dimensionless density of lubricant, ρ / ρ_0

β thermal expansivity of lubricant (K^{-1})

γ temperature-viscosity coefficient of lubricant (K^{-1})

σ dimensionless standard deviation of the measured error

7. Acknowledgments

8. References

Sternlicht, B., Lewis, P. & Flynn, P. (1961). Theory of lubrication and failure of rolling con tacts, *ASME J. Basic Eng.*, 83, pp. 213-226.

Ghosh, M. K. & Hamrock, B. J. (1985). Thermal elastohydrodynamic lubrication of line contacts, *Trans. ASLE 28 (2)*, pp. 159-171.

Salehizadeh, H. & Saka, N. (1991). Thermal non-Newtonian elastohydrodynamic lubrication of rolling line contacts, *ASME J Tribol.*, 113, pp. 481-491.

Lee, R. T. & Hsu, C. H. (1993). A fast method for the analysis of thermal-elastohydrodynamic lubrication of rolling/sliding line contacts, *Wear*, 166, pp. 107-117.

Zhu, D. & Wen, S. (1984). A full numerical solution of the thermal elastohydrodynamic lubrication problem of elliptic contacts, *ASME J. Lubrication Technology*, 106, pp. 246-254.

Kim, K. H. & Sadeghi, F. (1992). Three-dimensional temperature distribution in EHD lubrication: Part I -circular contact, *ASME J Tribol.*, 114, 32-41.

Lee, R. T., Hsu, C. H., Kuo, & W. F. (1995). Multilevel solutuion for thermal elastohydrodynamic lubrication of rolling/sliding circular contacts, *Tribol. Int.*, 28(8), pp. 541-552.

Cheng, H. S. & Orcutt, F. K. (1965). A correlation between the theoretical and experimental results on the elastohydrodynamic lubrication of rolling and sliding contacts, *Proc. Instn Mech. Engrs, Part B: J. Engineering Manufacture*, 180, pp. 158–168.

Safa, M. M. A., Anderson, J. C., & Leather, J. A. (1982). Transducers for pressure, temperature and oil film thickness measurement in bearings, *Sens. Actuators*, 3, pp. 119–128.

Kannel, J. W., Zugaro, F. F., & Dow, T. A. (1978). A method for measuring surface temperature between rolling/sliding steel cylinders, *Trans. ASME J. Lubr. Technol.*, 100, pp. 110–114.

Turchina, V., Sanborn, D. M., & Winer, W. O. (1974). Temperature measurements in sliding elastohydrodynamic point contacts, *Trans. ASME J. Lubr. Technol.*, 96, pp. 464–471.

Ausherman, V. K., Nagaraj, H. S., Sanborn, D. M., & Winer, W. O. (1976). Infrared temperature mapping in elastohydrodynamic lubrication, *Trans. ASME J. Lubr. Technol.*, 98, pp. 236–243.

K. Yagi1 ⌐, K. Kyogoku, and Nakahara T. (1996). Experimental investigation of effects of slip ratio on elastohydrodynamic lubrication film related to temperature distribution in oil films, *Proc. IMechE Vol. 220 Part J: J. Engineering Tribology*, pp. 102-112.

Yagi, K., Kyogoku, K. & Nakahara, T. (1997). Relationship Between Temperature Distribution in EHL Film and Dimple Formation, *Transactions of the ASME*, pp. 412-418.

Cameron, A. & Gohar, R. (1966). Theoretical and experimental studies of the oil fim in lubricated point contact, *Proc. R. Soc., Ser. A*, 291, pp. 520-536.

Foord, C. A., Hammann, W. C. & Cameron, A. (1968). Evaluation of lubricants using optical elastohydrodynamics, *ASLE Trans.*, 11(1), pp. 31-43.

Johnston, G. J., Wayte, R. & Spikes, H. A. (1991). The measurement and study of very thin lubricant films in concentrated contacts, *STLE Tribology Trans.*, 34(2), pp. 187-194.

Gustafsson, L., Hoglund, E. & Marklund, O. (1994). Measuring lubricant film thickness with image analysis, *Proc. Instn. Mech. Engrs., Part(J), J. of Eng. Tribology*, 208, pp. 199-205.

Yang, P., Qu, S., Kaneta, M. & Nishikawa, H. (2001). Formation of steady Dimples in point TEHL contacts, *ASME, J. of Tribology*, 123, pp.42-49.

Marklund, O. (1998). A pseudo-phase stepping approach to interferometric measurements, *TULEA:09 Lulea Univ. of Tech.*, S-97187 Lulea, Sweden.

Luo, J., Wen, S. & Huang, P. (1996). Thin Film Lubrication Part I: Study on the Transition between EHL and Thin Film Lubrication Using a Relative Optical interference Intensity Technique, *Wear*, 194, pp. 107-115

Hartl, M., Krupka, I., Poliscuk, R. & Liska, M. (1999). An Automatic System for Real-Time Evaluation of EHD Film Thickness and Shape Based on the Colorimetric Interferometry, *Trib. Trans.*, 42, 2, pp303-309.

Paul, G. R. & Cameron, A. (1972). A high-pressure microviscometer based on refractive index, *Proc. R. Soc., Ser. A*, 331, pp. 171-184.

Wong, P., Lingard, L. S. & Camerson, A. (1992). The high pressure impact microviscometer, *STLE Tribology Trans.*, 35(3), pp. 500-508.

Astrom, H. & Venner, C. H. (1994). Soap thickener induced local pressure fluctuations in a grease lubricated elastohydrodynamic point contact, *Proc. Instn. Mech. Engrs., Part(J), J. of Eng. Tribology*, 208, pp. 191-198.

Östensen, J. O., Larsson, R. & Venner, C. H. (1996) Determination of viscosity and pressure in an elastohydrodynamic rolling contact by using optical interferometry: a theoretical study, *Proc. Instn. Mech. Engrs., Part(J), J. of Eng. Tribology*, 210, pp. 259-268.

Lee, R. T., Chu, H. M. & Chiou, Y. C. (2002). Inverse approach for calculating pressure and viscosity in elastohydrodynamic lubrication of line contacts, *Tribology International*, Vol. 35, pp. 809-817.

Yang, C. Y. (1998). A linear inverse model for the temperature-dependent thermal conductivity determination in one-dimensional problems, *Applied Mathematical Modelling*, 22, pp. 1-9.

Dowson, D. & Higginson, G. R. (1966). Elastohydrodynamic Lubrication, *Pergamon Press*, pp. 88-92.

Roelands, C. J. A., Vlugter, J. C. & Watermann, H. I. (1963). The viscosity temperature pressure relationship of lubricating oils and its correlation with chemical constitution, *ASME Journal of Basic Engineering*, pp. 601-606.

Carslaw, H. S. & Jaeger, J. C. (1959). *Conduction of Heat in Solids*, Oxford University Press.
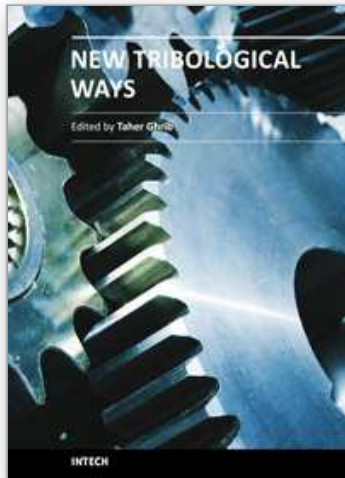
New Tribological Ways

Edited by Dr. Taher Ghrib

This book aims to recapitulate old information's available and brings new information's that are with the fashion research on an atomic and nanometric scale in various fields by introducing several mathematical models to measure some parameters characterizing metals like the hydrodynamic elasticity coefficient, hardness, lubricant viscosity, viscosity coefficient, tensile strength .... It uses new measurement techniques very developed and nondestructive. Its principal distinctions of the other books, that it brings practical manners to model and to optimize the cutting process using various parameters and different techniques, namely, using water of high-velocity stream, tool with different form and radius, the cutting temperature effect, that can be measured with sufficient accuracy not only at a research lab and also with a theoretical forecast. This book aspire to minimize and eliminate the losses resulting from surfaces friction and wear which leads to a greater machining efficiency and to a better execution, fewer breakdowns and a significant saving. A great part is devoted to lubrication, of which the goal is to find the famous techniques using solid and liquid lubricant films applied for giving super low friction coefficients and improving the lubricant properties on surfaces.

How to reference

In order to correctly reference this scholarly work, feel free to copy and paste the following:

INTECH
open science | open minds